CrystEngComm

UdP MOFs

ROYAL SOCIETY
OF CHEMISTRY

PAPER
Giulio Bresciani *et al.*
Synthesis and structural characterisation of Cu^{II}-based
MOFs constructed by combining functionalised
1,4-bis(1*H*-imidazol-1-Yl)benzene ligands with copper sulfate

Check for updates

Synthesis and structural characterisation of Cu(II)-based MOFs constructed by combining functionalised 1,4-bis(1H-imidazol-1-Yl)benzene ligands with copper sulfate†

Giulio Bresciani, [iD] *[ab] Massimo Guelfi, [iD][ab] Melodj Dosa, [iD][c] Virginia Guiotto, [iD][c] Valentina Crocellà, [iD][c] Marco Lessi [iD][ab] and Marco Taddei [iD] *[ab]

Anion-pillared metal–organic frameworks (APMOFs) are a class of coordination polymers in which divalent anions connect two adjacent layers of a 2D network generated by neutral ligands and cationic metal centres. This class of MOFs is commonly composed by materials built using pyridine-based ligands and octahedral fluorinated anions as linear pillars. Only recently, the use of nitrogen based five-membered ring ligands and/or tetrahedral anions, such as sulfate, has been reported. The combination of 1,1′-(2-(trifluoromethyl)-1,4-phenylene)bis(1H-imidazole) (**bibCF₃**) ligand with copper(II) sulfate generates a 2D MOF (**UdP-20**) of minimal formula [CuSO₄(**bibCF₃**)₁.₅]·3H₂O. **UdP-20** possesses a square lattice (**sql**) topology in which the copper sulfate dimer molecular building block acts as 4-connected nodes and exhibits flexibility, transitioning to a closed pore phase (**UdP-20-cp**) upon heating. The use of different functionalised **bib** ligands allowed us to obtain three new examples of APMOFs: **UdP-21** with 1,1′-(2-chloro-1,4-phenylene)bis(1H-imidazole) (**bibCl**), **UdP-22** with 1,1′-(2-methyl-1,4-phenylene)bis(1H-imidazole) (**bibMe**) and **UdP-23** with 1,1′-(2-methoxy-1,4-phenylene)bis(1H-imidazole) **bibOMe**. All these materials possess 2D layers connected to each other by bridging sulfate anions leading to an overall 3D anion pillared framework. All the herein reported materials were characterised by elemental analysis, thermogravimetric analysis, and powder and single crystal X-ray diffraction. Moreover, their CO₂ adsorption behaviour was investigated, revealing results in alignment with what is already reported in the literature for similar materials in the case of **UdP-20**, while **UdP-21**, **UdP-22** and **UdP-23** exhibited moderate CO₂ adsorption, due to transition to denser phases upon activation.

Introduction

Porous coordination networks (PCNs) are a class of sorbents constructed by coordination of inorganic and/or organic ligands to metal ions generating a porous network. PCNs are promising materials that could be used in catalysis, in volatile organic compound (VOC) capture and in gas separation/storage, *e.g.* carbon dioxide, methane, and water vapor.[1–7] Most PCNs are built from metal ions or clusters paired with anionic organic linkers, classifying them as metal–organic frameworks (MOFs).[8–10] However, when neutral ligands are employed, the inorganic counteranions can significantly influence the topology of the resulting structure.[11,12] For instance, divalent inorganic anions can serve as ditopic linkers, connecting adjacent layers by coordinating cationic metal nodes within two-dimensional (2D) metal–organic layers, resulting in the formation of anion-pillared metal–organic frameworks (APMOFs).[13,14] APMOFs can be prepared using either linear pillars, typically octahedral fluorinated anions (*e.g.*, SiF₆²⁻, TiF₆²⁻, NbOF₅²⁻, TaOF₅²⁻, WO₂F₄²⁻),[13–17] or angular pillars, such as CrO₄²⁻, MoO₄²⁻, WO₄²⁻, PO₄³⁻ and SO₄²⁻.[13,14,18–20] It is important to note that the choice of the counteranion influences not only the framework's connectivity, but also the strength of the metal-pillar bonds, thereby influencing the overall stability of the resulting

[a] Dipartimento di Chimica e Chimica Industriale, Università di Pisa, Via G. Moruzzi 13, I-56124 Pisa, Italy. E-mail: giulio.bresciani@dcci.unipi.it, marco.taddei@unipi.it

[b] Centro per l'Integrazione della Strumentazione Scientifica dell'Università di Pisa (C.I.S.U.P.), Università di Pisa, Pisa, Italy

[c] Dipartimento di Chimica, Centro Interdipartimentale NIS, Unità di Ricerca INSTM, Università di Torino, Via G. Quarello 15, I-10135 and Via P. Giuria 7, I-10125 Torino, Italy

APMOF. Despite the outstanding gas adsorption and separation properties demonstrated by some APMOFs, such as the SIFSIX family,[21–25] the use of fluoride-based anions poses challenges that include the potential risk of HF exposure during the synthesis of inorganic anions or during the thermal decomposition of the material.[26] The use of environmentally friendly and abundant sulfate anions as the pillar can represent a valid alternative to fluorinated anions. To date, several MOFs having sulfate anions as pillars have been published in the literature, but the adsorption properties for only a few of them have been investigated.[19,21,27–34] In particular, interesting results in term of gas separation were obtained using a new sulfate APMOF, referred to as SOFOUR-1-Zn, built employing tetra(4-pyridyl)benzene (TEPB) as the organic linker and Zn^{II} as the metal node.[19] Since the publication of this work, three other members of this family of APMOFs were reported to be active in C_2H_2/CO_2 separation: SOFOUR-TEPE-Zn (TEPE = 1,1,2,2-tetra(pyridin-4-yl)ethene),[20] SOFOUR-DPDS-Ni (DPDS = 4,4′-dipyridyldisulfide)[31] and SOFOUR-2-Zn having enmepy (N^1,N^2-bis(pyridin-4-ylmethyl) ethane-1,2-diamine) as the ligand.[32,33] Almost all the SOFOUR and most of the APMOFs reported are typically constructed using a pyridine-based ligand. In comparison, there are relatively few examples in the literature of such materials incorporating N-based five-membered ring ligands, such as imidazoles, pyrazoles, triazoles, or tetrazoles.[5,13,14,35–37] For instance, the APMOF constructed using 1,4-bis(1-imidazolyl) benzene (**bib**) as a ligand in combination with $CuSiF_6$, named SIFSIX-23-Cu, exhibits a unique *cis*-bridging coordination mode of hexafluorosilicate anions.[23,24] Moreover, this material displays a flexible framework whose phase switching can be triggered by CO_2 adsorption. The reversible transformation observed is attributed to the low rotational barrier of the **bib** ligand.[3,23,38–40] When the benzene ring in the linker was replaced with a pyridine, the resulting flexible coordination network, SIFSIX-23-Cu^N, displayed a shape-memory effect.[22] The first two materials prepared combining **bib** or a functionalised **bib** ligand (1,4-bis(1-imidazolyl)naphthalene = **bin**) with copper sulfate were recently reported by Zaworotko and co-workers.[41] Both these materials showed a 2D square lattice network with a peculiar sulfate dimer molecular building block. In particular, the use of the more sterically hindered **bin** allowed obtaining a MOF that exhibits high selectivity for C_2H_2 over CO_2 and C_2H_4.

Given our recent interest in the study of copper-based MOFs using **bib** as a linker,[42] we report herein our studies on the synthesis, characterisation and adsorption properties of new MOFs employing four different 1,4-bis(1-imidazolyl) benzene ligands functionalised on the benzene ring and copper sulfate as the inorganic salt.

Results and discussion

Layering a methanolic solution of 1,1′-(2-(trifluoromethyl)-1,4-phenylene)bis(1*H*-imidazole) (**bibCF₃**) on a water/ethylene glycol solution of $CuSO_4$ (for further details see the

Experimental section) afforded blue crystals of **UdP-20** (UdP stands for Università di Pisa) suitable for single crystal X-ray analysis. **UdP-20** crystallises in the triclinic $P\bar{1}$ space group with the following lattice parameters: a = 9.9888(5) Å, b = 11.4316(5) Å, c = 12.6577(7) Å, α = 104.810(2)°, β = 94.908(2)°, γ = 102.704(2)°, and volume = 1347.6(1) Å^3 (for further details see Table S1†). The asymmetric unit consists of one Cu^{II} atom, one sulfate anion, one **bibCF₃** ligand (named A) and one half **bibCF₃** ligand (named B) whose centre of mass lies on an inversion centre (Fig. 1a). The former **bibCF₃** adopts an *antiperiplanar* conformation[43] (Cu–N–N–Cu torsion angle 172.9°, Fig. S1†) with a dihedral angle between planes designed by the imidazoles of 8.3° (Fig. S2†). The dihedral angles between the benzene ring plane and the imidazole planes are 46.5° and 38.5°, respectively (Fig. S3†). Moreover, the CF_3 group on the **bibCF₃** ligand A is subjected to positional disorder with a slight preference for the *ortho* position respect to N4 (freely refined occupancy of 56%, Fig. S4†). Also **bibCF₃** ligand B adopts an *antiperiplanar* conformation[43] with a Cu–N–N–Cu torsion angle of 180.0° (Fig. S5†) and with the two imidazole rings lying on parallel planes that form a dihedral angle with the benzene ring plane of 49.9° (Fig. S6†). As already observed for $CuSO_4(\mathbf{bib})_{1.5}$,[41] the structure possesses a copper sulfate dimer molecular building block (MBB) in which the Cu atoms are bridged by two sulfate anions bonding with a
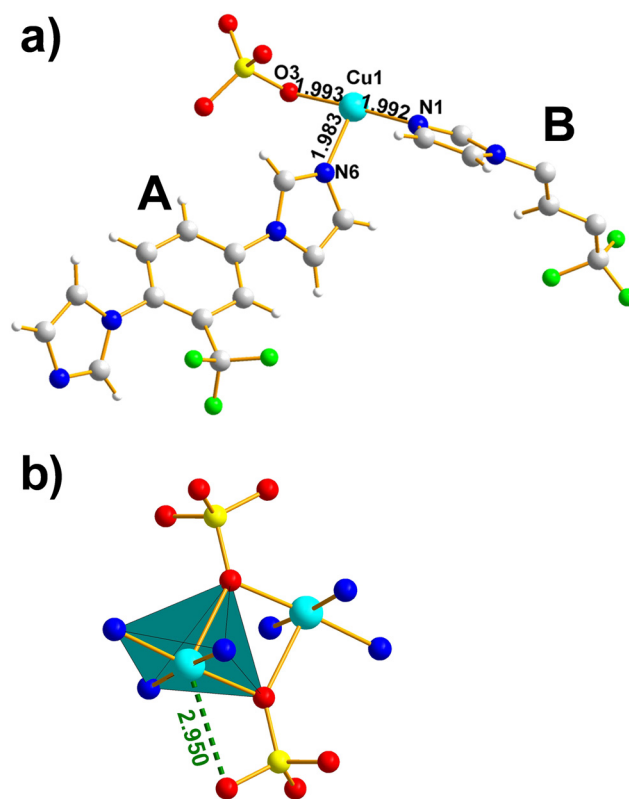

Fig. 1 Asymmetric unit and selected bond distances (a) and coordination environment of copper (b) in **UdP-20**. Nomenclature A and B refers to crystallographic independent **bibCF₃** ligands in the asymmetric unit. Colour code: Cu, cyan; F, green; N, blue; C, grey; S, yellow; O, red; H, white.

(μ-κ^1O)-coordination mode forming a Cu_2O_2 ring with its centre of mass located on an inversion centre (Fig. 1b). Each Cu is pentacoordinated in a distorted square pyramidal geometry with two positions occupied by the sulfate oxygen atoms and three position occupied by the imidazole nitrogen atoms (Fig. 1b). The base of the pyramid presents an open metal site with the nearest sulfate oxygen atom at 2.950 Å (Fig. 1b).

Due to the orientation of the **bibCF₃** ligands, the overall structure of **UdP-20** possesses a 2D square lattice (**sql**) topology in which the $CuSO_4$ MBB serves as a 4-connected node that binds other dimers through one ligand in a direction and through two parallel ligands forming a "double wall" (Fig. 2a). The structure has 19.9% of void space thanks to 1D channels running along the *c* axis (Fig. 2b). Layers present a sort of zig-zag conformation (Fig. 2c) with the interlayer distance (7.13 Å, Fig. S7†) that resemble more the distance observed in $CuSO_4$(**bin**)$_{1.5}$ (7.32 Å) than in $CuSO_4$(**bib**)$_{1.5}$ (4.99 Å).[41]

While bulk syntheses of **UdP-20** using a water/methanol mixture at 298 K or 333 K did not allow us to isolate the same material obtained in single crystalline form (Fig. S8†), the use of a water/acetonitrile mixture at 353 K (for further details see the Experimental section) enabled the formation of the desired phase (Fig. 3a). Elemental analysis (Experimental section) and TGA (Fig. S9†) on the freshly synthesised powder are coherent with a MOF of formula [$CuSO_4$(**bibCF₃**)$_{1.5}$]·$3H_2O$. To evaluate the stability of the structure, PXRD patterns were registered after heating **UdP-20** in an oven at 353 K for 2 hours, revealing the transformation of this material to another phase, named **UdP-20-cp** (closed pores, Fig. 3a). Indexing the phase allowed us to reveal that the material probably preserves the connectivity and the topology of **UdP-20**, maintaining the triclinic $P\bar{1}$ space group with a contraction of the cell volume of 9%. Lattice parameters of **UdP-20-cp** were found to be: a = 9.423(2) Å, b = 11.460(2) Å, c = 12.735(4) Å, α = 70.93(1)°, β = 69.03(1)°, γ = 79.553(7)°, and volume = 1210.47 Å³ (Fig. S10†). Noteworthy, **UdP-20-cp** remains stable for months if stored in the presence of moist air while the exposure of the material to acetone vapours allowed restoring the same phase of **UdP-20** in 15 hours (Fig. S11†), confirming the reversibility of the process. Similar transformations were already observed in [$CuSO_4$(**bib**)$_{1.5}$] and [$CuSO_4$(**bin**)$_{1.5}$] using single crystals.[41] Unfortunately, the attempts to achieve the phase transition on **UdP-20** single crystals failed due to the loss of crystallinity during the transformation.

The gas sorption properties of **UdP-20** were initially investigated by evaluating the N_2 adsorption at 77 K on a sample activated at 353 K under vacuum to achieve a complete transformation to **UdP-20-cp**. Unfortunately, the material seems to be not porous to nitrogen considering the very low adsorption uptake (<3 cm³ g⁻¹ STP) (Fig. S12†). On the other hand, the material displays a type I isotherm for CO_2 adsorption at 273 K on an **UdP-20** sample activated as described above. The maximum uptake showed by **UdP-20-cp** is 0.98 mmol g⁻¹ at 1.1 bar (Fig. 3b). These results are in accordance with what was already observed for [$CuSO_4$(**bib**)$_{1.5}$][41] revealing that the substitution of a hydrogen atom with a CF_3 group on the benzene ring of the ligand did not affect the adsorption properties of this kind of 2D materials.

With the aim of further expanding the family, we applied the same crystallisation method described for **UdP-20** using three more substituted ligands, *i.e.*, **bibCl** (**UdP-21**), **bibMe** (**UdP-22**), **bibOMe** (**UdP-23**). All these materials crystallise in the triclinic $P\bar{1}$ space group with lattice parameters summarised in Table S1† and, surprisingly, none of these structures resembles the **UdP-20** framework. The asymmetric units of **UdP-21** and **UdP-22** consist of two Cu^{II} centres sitting on an inversion centre, a sulfate anion and two **bibX** (X = Cl or Me) ligands (named A and B, Fig. 4a and b). The **bibX** type A ligand adopts a *synclinal* conformation[43] (Cu–N–N–Cu torsion angle around 40°, Fig. S13†) with a dihedral angle between planes designed by imidazole rings around 69° (Fig. S14†). The other **bibX** ligand present in the asymmetric unit (named B) also possesses a *synclinal* conformation[43] (Cu–N–N–Cu torsion angle around −89°, Fig. S15†) with a dihedral
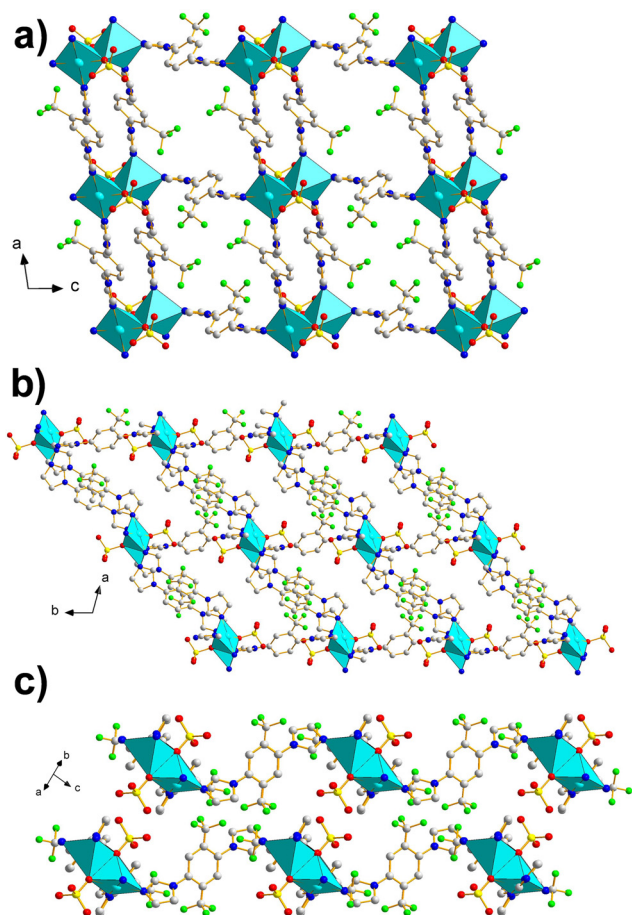

Fig. 2 View of a **UdP-20** monolayer along the *b* axis (a) and the *c* axis (b). Side view of two corrugated adjacent layers (zig-zag conformation) in **UdP-20** (c). Colour code: Cu, cyan; F, green; N, blue; C, grey; S, yellow; O, red. Hydrogen atoms have been omitted for clarity.
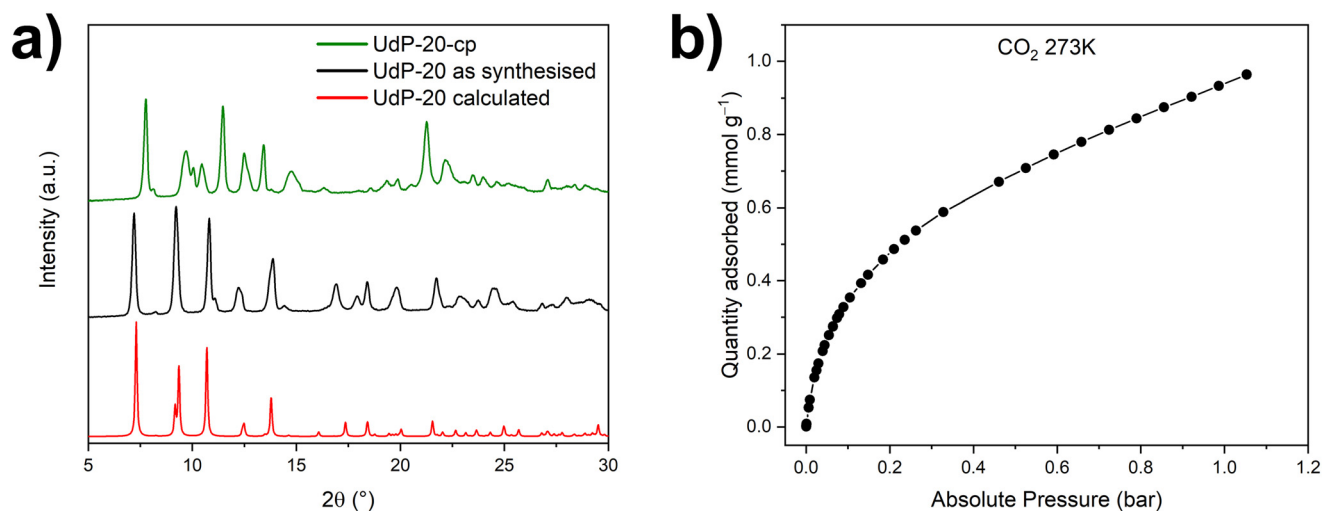
Fig. 3 PXRD pattern comparison between **UdP-20** calculated (red), **UdP-20** as synthesised and **UdP-20** after the activation process (**UdP-20-cp**, green) (a). CO$_2$ isotherm at 273 K registered on **UdP-20-cp** (b).
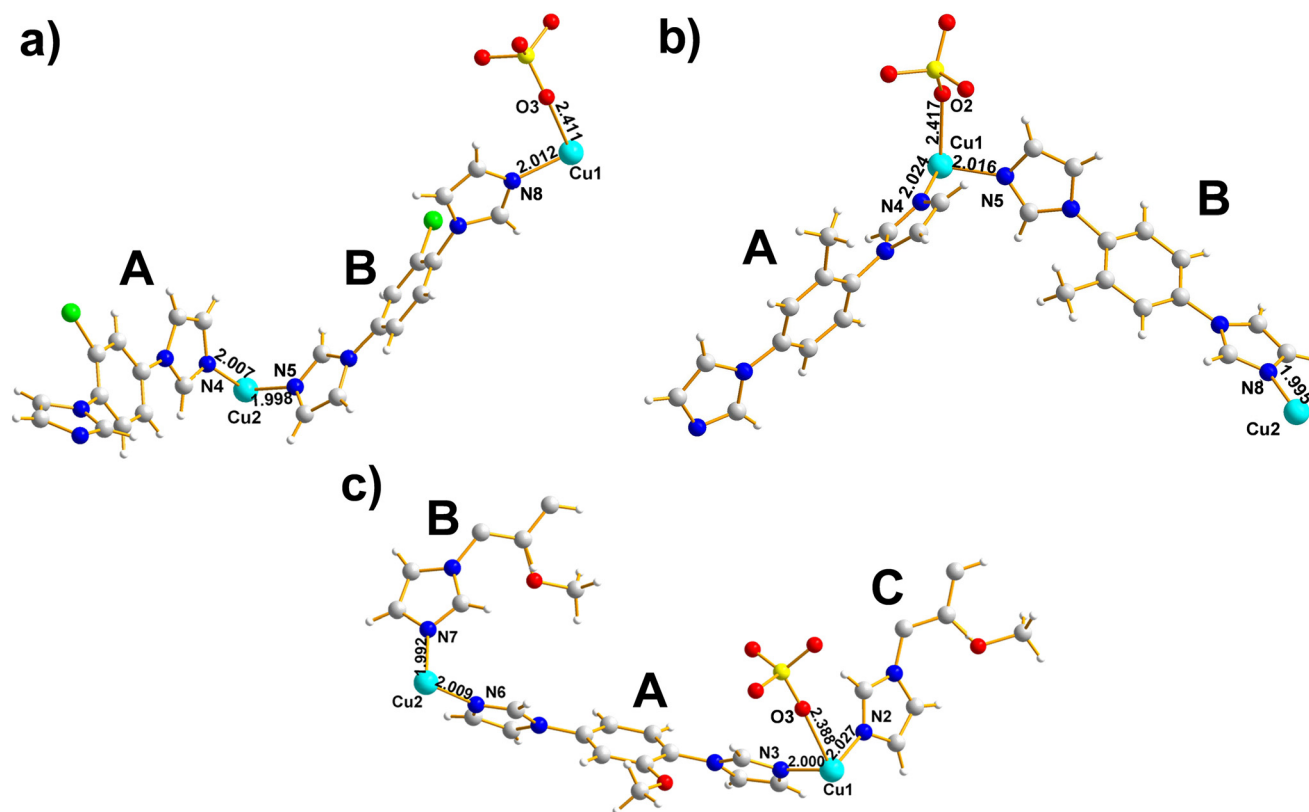

Fig. 4 Asymmetric units and selected distances of **UdP-21** (a), **UdP-22** (b) and **UdP-23** (c). Nomenclature A, B and C refers to crystallographic independent **bibX** ligands in the asymmetric units. Colour code: Cu, cyan; Cl, green; N, blue; C, grey; S, yellow; O, red, H, white.

angle between planes designed by imidazole rings of *ca.* 86° (Fig. S16†). Different from **UdP-21** and **UdP-22**, **UdP-23** possesses an asymmetric unit composed by one **bibOMe** ligand (named A) and two half ligands (named B and C, respectively) whose centres of mass are sitting on an inversion centre (Fig. 4c). The type A **bibOMe** ligand exhibits

a *syn* conformation (Cu–N–N–Cu torsion angle 2.2°, Fig. S17†) with the imidazole rings lying on almost parallel planes (dihedral angle between planes 0.3°, Fig. S18†). On the other hand, the two half ligands (named B and C) in **UdP-23** possess an *anti* conformation (Cu–N–N–Cu torsion angle 180.0°, Fig. S19†) with the two imidazoles rings lying on

parallel planes close to each other (dihedral angle 0.0°, distance 0.39 Å, Fig. S20†).

Notably, **UdP-23** exhibits disorder on sulfate anions and on **bibOMe** ligands. The former was principally disordered on two positions and its occupancy was freely refined with a preference of 61% for one of the two positions (Fig. S21†). The disorder of the functional group on ligands named B and C can be attributable to the proximity of the symmetry element, while the OMe group on the ligand A is subjected to positional disorder due to the different coordination direction of the ligand, with a slight preference for the proximity to Cu1 (Fig. 4c; freely refined occupancy of 58%, Fig. S22†).

In all the materials, the coordination environment of both Cu atoms in the asymmetric unit is formed by four imidazoles and two sulfate ions, resulting in hexacoordinated metal centres in a distorted octahedral geometry with the sulfate ions coordinated in mutual *trans* position (Fig. 5a and S23†). Moreover, all these materials exhibit the same topology, where each Cu centre is connected to other four Cu atoms through **bibX** ligands, thus acting as a 4-connected node in a **sql** grid topology with corrugated layers (Fig. 5b and c). The 2D layers are connected to each other by coordination of bridging sulfate anions to Cu atoms, above and below the layers leading to an overall 3D anion pillared framework (Fig. 5d). Therefore, **UdP-21**, **UdP-22** and **UdP-23** can be accounted as new members of the SOFOUR family of materials.[14,19] The use of SQUEEZE[44] to remove diffused and disordered solvent in the pores was necessary to properly refine the crystal structures. Therefore, **UdP-21**, **UdP-22** and **UdP-23** showed 34.7%, 34.3% and 22.6% of void space, respectively, thanks to the 1D channel running along the *b* axis.

Bulk synthesis of **UdP-21**, **UdP-22** and **UdP-23** can be performed by mixing a water solution of $CuSO_4$ with a methanolic solution of the selected ligand at room temperature. Light blue powders, whose PXRD patterns were in good agreement with the calculated from single crystal structures (Fig. 6a–c), were obtained. Moreover, elemental analysis and TGA (Fig. S24†) performed on powder samples confirm that all these MOFs have the general formula $[CuSO_4(\textbf{bibX})_2]\cdot Y H_2O$, with an *Y* amount of physisorbed water which depends on the material (see the Experimental section).

Several attempts to obtain a similar anion pillared structure using the **bibCF₃** ligand were conducted, even using a large excess (5 equivalents) of **bibCF₃**, trying to access the 2:1 stoichiometry exhibited by **UdP-21**, **UdP-22** and **UdP-23**. However, the same **UdP-20** phase was consistently obtained.

The new SOFOUR materials were studied as gas sorbents exhibiting interesting properties, in particular in separation of light hydrocarbons and CO_2.[19,20,31,33] As a preliminary investigation, we evaluated the adsorption properties of the newly prepared sulfate-pillared MOFs. As observed for **UdP-20**, **UdP-21**, **UdP-22** and **UdP-23** are not porous through N_2 measured at 77 K (Fig. S25†), while

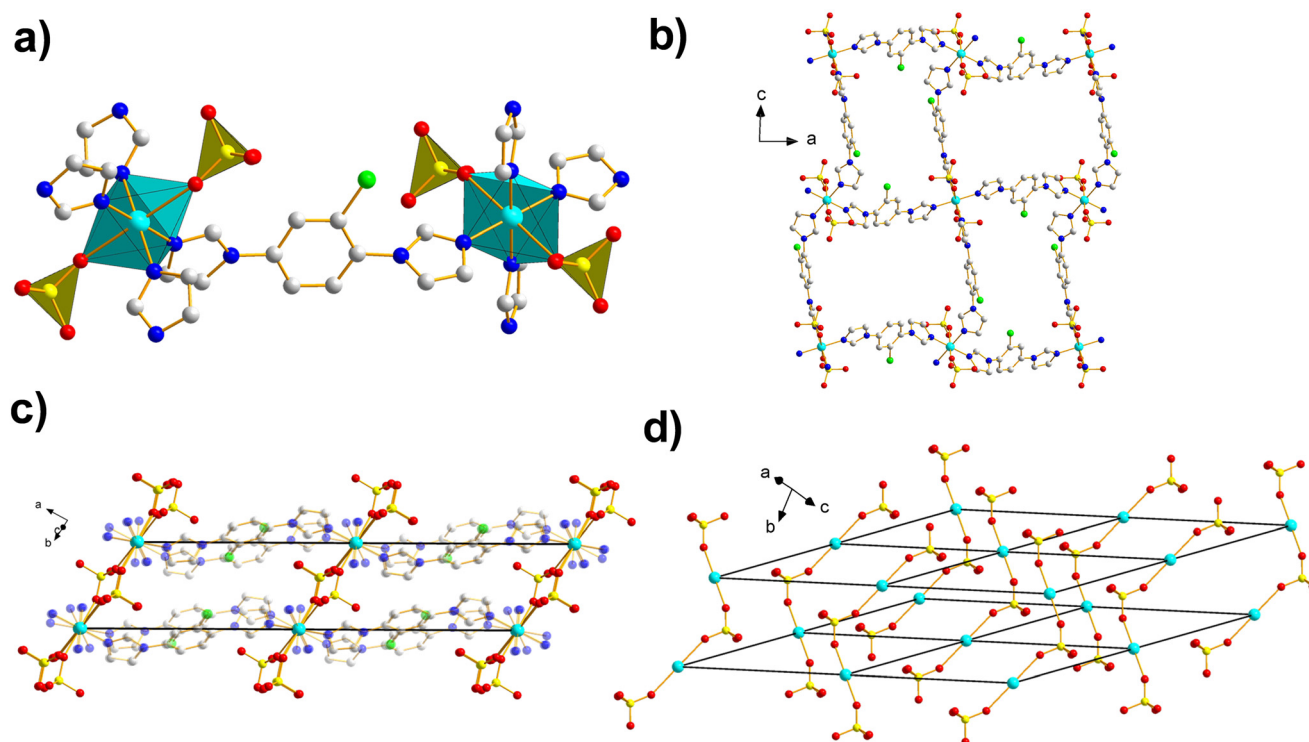**Fig. 5** **UdP-21**: copper and sulphur coordination environments (a), view of a monolayer along the *b* axis (b), view of two adjacent layers from two different perspectives (c) and (d). In (c) and (d), the connection through ligands between Cu atoms was represented by a black line. Colour code: Cu, cyan; Cl, green; N, blue; C, grey; S, yellow; O, red. Hydrogen atoms have been omitted for clarity.
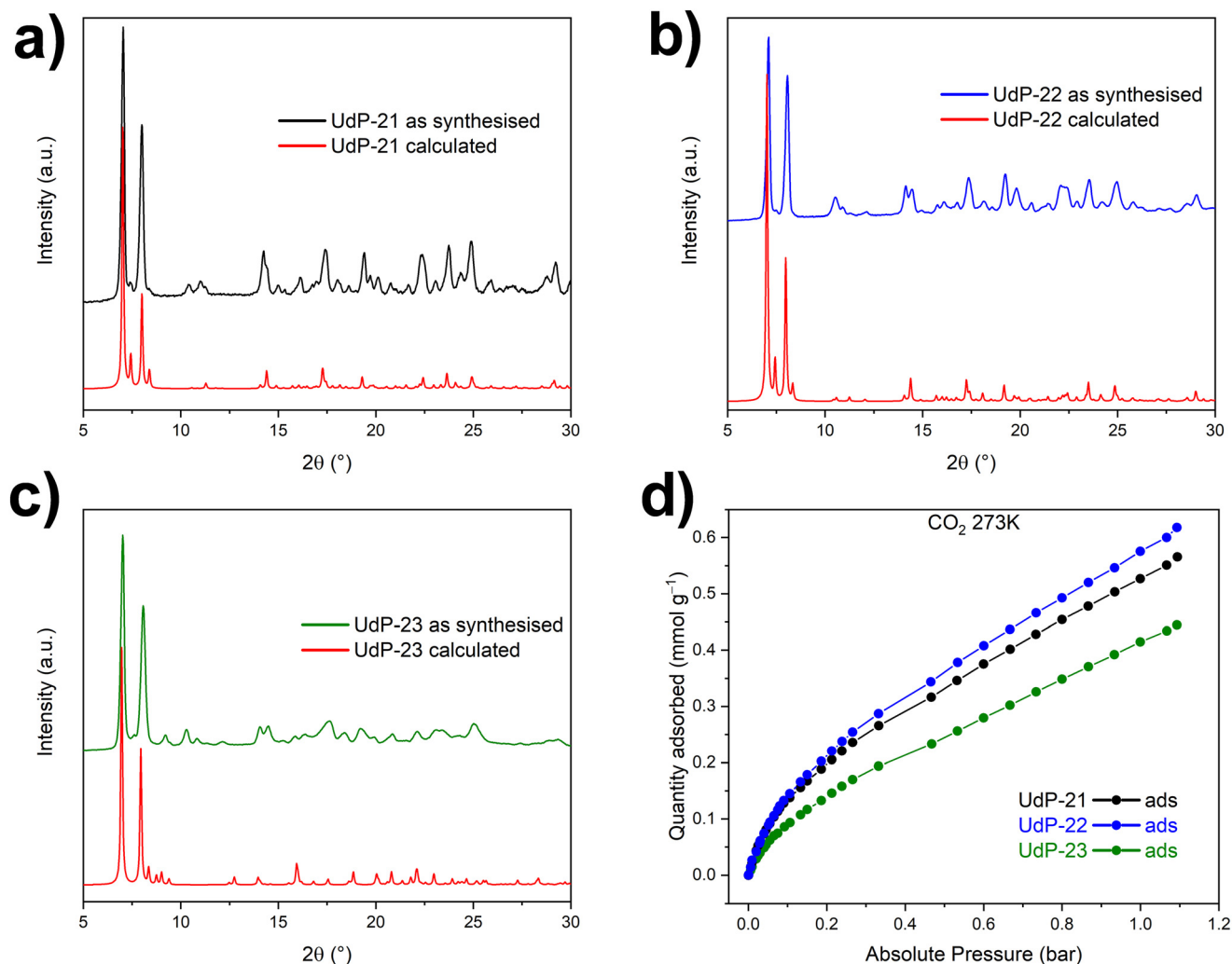
Fig. 6 Experimental and calculated PXRD patterns (a)–(c) and CO_2 isotherms at 273 K (d) of **UdP-21**, **UdP-22** and **UdP-23**.

they exhibit type I CO_2 adsorption isotherms at 273 K, with a low gas adsorption capacity (Fig. 6d) compared to **UdP-20** and to other SOFOUR MOFs reported in the literature.[19,20,31] Specifically, **UdP-21** and **UdP-22** exhibit similar CO_2 adsorption at 1 bar with maximum uptakes of 0.57 mmol g^{-1} and 0.62 mmol g^{-1}, respectively, while **UdP-23** displays an adsorption of 0.44 mmol g^{-1} at 1 bar.

In order to evaluate the effect of the activation process, PXRD patterns were collected on **UdP-21**, **UdP-22** and **UdP-23**, after heating at 353 K under vacuum to replicate the activation procedure (Fig. S26–S28†). **UdP-21** and **UdP-22** showed a loss of long range order after thermal treatment, with unaltered structure connectivity. The original PXRD patterns can be restored after exposure of the powder to moist air for several days (14 days for **UdP-21**; 2 days for **UdP-22**). On the other hand, **UdP-23** showed a phase transition during the activation process and thus variable temperature powder X-ray diffraction (VTPXRD) patterns were also registered showing a double step phase transition first at 393 K and then at 433 K. After exposure of the powder to moist air for 18 hours, the intermediate phase

was restored (Fig. S28†) and remained stable even after one month. Unfortunately, due to the limited crystallinity of these new phases, we were not able to index their powder patterns.

Conclusions

Moved by the desire to prepare pillared materials and study the influence of different functional groups on the benzene ring of **bib** ligand on the structural motif, we combined 1,1′-(2-(trifluoromethyl)-1,4-phenylene)bis(1*H*-imidazole) (**bibCF₃**) ligand with copper(II) sulfate obtaining a 2D material (**UdP-20**) in which the 4-connected nodes of each layer are composed of a dimeric Cu_2O_2 ring formed by two Cu atoms and two (μ_2-η_2)-sulfate anions. Heating the **UdP-20** powder sample allowed the transition to a closed pore phase (**UdP-20-cp**), which exhibit a reduced cell volume of 9%. Notably, exposing **UdP-20-cp** to acetone vapours successfully restored the original **UdP-20** phase, demonstrating the reversibility of the process. CO_2 adsorption properties of **UdP-20** were also investigated at 273 K, displaying a type I isotherm with

modest amount of gas adsorbed. Structural results and CO_2 adsorption properties are in alignment with a similar 2D material previously reported in the literature, *i.e.* $CuSO_4(\textbf{bib})_{1.5}$.

Following the same crystallization method employed for **UdP-20**, other functionalised **bib** ligands were used, *i.e.*, 1,1′-(2-chloro-1,4-phenylene)bis(1*H*-imidazole) (**bibCl**), 1,1′-(2-methyl-1,4-phenylene)bis(1*H*-imidazole) (**bibMe**) and 1,1′-(2-methoxy-1,4-phenylene)bis(1*H*-imidazole) (**bibOMe**). Combination of these ligands with $CuSO_4$ afforded three new isostructural MOFs, **UdP-21**, **UdP-22** and **UdP-23**, with the general formula $[CuSO_4(\textbf{bibX})_2]\cdot y H_2O$. In contrast with what observed for **UdP-20**, these materials possess a typical anion pillared framework in which 2D layers, formed by cationic metals (4-connected nodes) and ligands, are connected to each other by coordination of anions (SO_4^{2-} in these cases) to the metal centres revealing the functional group influence on the structural topology. Therefore, **UdP-21**, **UdP-22** and **UdP-23** can be accounted as the first non-pyridine based members of the SOFOUR family. Adsorption properties of these new sulfate-pillared MOFs were preliminarily investigated exhibiting type I CO_2 isotherms with a low amount of sorbed gas probably due to a loss of crystallinity (for **UdP-21** and **UdP-22**) and to a phase transition (for **UdP-23**) during the activation process.

Experimental

Materials and methods

Reactants and solvents were purchased from Alfa Aesar, Merck, Strem, FluoroChem or TCI Chemicals, and were of the highest purity available. The glass reaction vessels for the ligand synthesis were dried at 413 K prior to use, evacuated (10^{-2} mbar) and then filled with nitrogen. The ligand syntheses were conducted under N_2 atmosphere using standard Schlenk techniques by a slight modification of reported procedure.[45] Products were stored in air once isolated.

Gas chromatography flame ionisation detector (GC-FID) analysis was performed using a Nexis GC-2030 gas chromatograph (Shimadzu, Japan) equipped with a J&W DB-1 column (15 m × 0.25 mm × 0.25 μm, Agilent Technologies, USA).

^{1}H, ^{13}C and ^{19}F nuclear magnetic resonance (NMR) spectra were recorded on a Jeol JNM-ECZ400S instrument equipped with a Royal Broadband probe. Chemical shifts (expressed in parts per million) are referenced to the residual solvent peaks for ^{1}H and ^{13}C and to $CFCl_3$ as external standard for ^{19}F.[46]

Powder X-ray diffraction (PXRD) patterns were collected in the 5–35° 2θ range with a Rigaku MiniFlex 600C diffractometer using Cu Kα radiation (1.54056 Å). The X-ray tube was operated at a voltage of 40 kV and a current of 15 mA. Variable temperature powder X-ray diffraction (VTPXRD) patterns were obtained using the above-described diffractometer with a BTS500 benchtop heating stage (Anton

Paar). The sample was heated from 303 K to 433 K with a rate of 10 K min^{-1} and the sample was left at the desired temperature for 15 minutes before collecting the pattern.

CHNS elemental analyses were performed on a Vario MICRO cube instrument (Elementar).

TGA of samples were performed with a TA Instruments Thermo balance model Q5000IR using a heating rate of 5 °C min^{-1} in the temperature range of 303–973 K under air flow (20 mL min^{-1}). The sample amount was in the range 3.430–3.554 mg. Mass calibration was performed using certified mass standards, in the range 0–100 mg, supplied by TA Instruments. Temperature calibration was based on the Curie point of paramagnetic metals. A multi-point calibration with five Curie point reference materials (Alumel, Ni, Ni83%Co17%, Ni63%Co37%, and Ni37%Co63%) was performed.

N_2 adsorption isotherms were collected at 77 K on a Micromeritics 3Flex sorption analyser. The cooling bath was prepared using liquid nitrogen. CO_2 adsorption measurements were carried out on a Micromeritics ASAP 2020 analyser at 273 K. The temperature was kept constant thanks to a home-made patented glass coating cell[47] in which a coolant or heating fluid, connected to a thermostatic bath (JULABO F25), is recirculating. Prior to all sorption measurements, the sample (about 200 mg) was heated overnight at 353 K under vacuum (residual pressure 7 μbar).

Synthesis of bibX (X = CF$_3$, Me, Cl, OMe) ligands

General procedure. The selected 2-X-1,4-dibromobenzene derivative (*ca.* 15 mmol), imidazole (*ca.* 45 mmol), CuI (20 mol%) and K_2CO_3 (*ca.* 45 mmol) were placed in a 250 mL two neck round bottom flask, equipped with a reflux condenser. Three cycles of vacuum/N_2 were done and then 45 mL of anhydrous *N*,*N*-dimethylformamide (DMF) was added. The resulting reaction mixture was then heated to 423 K and stirred for 24–48 h. After cooling to room temperature, the mixture was diluted with 150 mL of a CH_2Cl_2/CH_3OH (1 : 1 v/v) mixture and filtered over a celite pad. Solvents were evaporated from the filtered organic layer and the residue was suspended in 150 mL of CH_2Cl_2. The suspension was transferred to a large separating funnel and washed twice with H_2O (2 × 250 mL). The organic layer was collected and then dried over $MgSO_4$. The solvent was evaporated at reduced pressure affording a solid that was purified by trituration (8 h) in hexane (80 mL).

Bulk synthesis of [CuSO$_4$(bibCF$_3$)$_{1.5}$]·3H$_2$O, UdP-20

A freshly prepared aqueous solution of $CuSO_4\cdot 5H_2O$ (0.03 M, 10 mL) was heated to 353 K and then added to a refluxing solution of **bibCF$_3$** in CH_3CN (0.06 M, 10 mL). The resulting mixture was stirred at 353 K for 4 hours and then cooled to room temperature. The solid obtained was centrifuged and washed with CH_3CN (10 mL) at 328 K for 1 hour and then with acetone (2 × 5 mL) for 20 minutes each portion. The light blue solid was dried in air overnight and then in the oven at 353 K for 20 minutes. Yield 140 mg (69%). Elemental

analysis found: C, 40.59; H, 3.45; N, 13.85; S, 5.05. Calcd. for [CuSO$_4$(**bibCF$_3$**)$_{1.5}$]·3H$_2$O: C, 38.42; H, 3.37; N, 14.59; S, 4.77.

Bulk synthesis of [CuSO$_4$(bibX)$_2$]·YH$_2$O (X = Me, Y = 9; X = Cl, Y = 8; X = OMe, Y = 7)

An aqueous solution of CuSO$_4$·5H$_2$O (0.3 M, 1.0 mL) was added dropwise to a methanolic solution of selected monosubstituted **bibX** (0.6 M, 1.0 mL). Instantaneous formation of a solid was observed. The mixture was vigorously stirred for 18 hours at room temperature and then the solid was washed with CH$_3$OH (2 × 3 mL) for 30 hours and with acetone (4 mL) for 20 minutes. The solid obtained was finally dried in air overnight and in an oven at 353 K for 20 minutes.

[CuSO$_4$(bibCl)$_2$]·8H$_2$O, UdP-21

From **bibCl** (150 mg, 0.61 mmol) and CuSO$_4$·5H$_2$O (76 mg, 0.30 mmol). Light blue solid. Yield 220 mg (79%). Elemental analysis found: C, 36.67; H, 4.19; N, 14.35; S, 3.86. Calcd. for [CuSO$_4$(**bibCl**)$_2$]·8H$_2$O: C, 36.35; H, 4.32; N, 14.13; S, 4.04.

[CuSO$_4$(bibMe)$_2$]·9H$_2$O, UdP-22

From **bibMe** (150 mg, 0.67 mmol) and CuSO$_4$·5H$_2$O (83 mg, 0.33 mmol). Light blue solid. Yield 232 mg (93%). Elemental analysis found: C, 40.24; H, 5.25; N, 14.44; S, 4.14. Calcd. for [CuSO$_4$(**bibMe**)$_2$]·9H$_2$O: C, 40.54; H, 5.50; N, 14.55; S, 4.16.

[CuSO$_4$(bibOMe)$_2$]·7H$_2$O, UdP-23

From **bibOMe** (150 mg, 0.62 mmol) and CuSO$_4$·5H$_2$O (78 mg, 0.31 mmol). Light blue solid. Yield 182 mg (76%). Elemental analysis found: C, 40.37; H, 4.87; N, 14.46; S, 4.15. Calcd. for [CuSO$_4$(**bibOMe**)$_2$]·7H$_2$O: C, 40.28; H, 5.07; N, 14.45; S, 4.14.

Crystallisation of UdP-20, 21, 22, 23

In a 15 × 160 mm test tube equipped with a screwcap, CuSO$_4$·5H$_2$O (23 mg, 0.09 mmol) was dissolved in 0.3 mL of water and then 6 mL of ethylene glycol was added. 3 mL of water buffer was layered on the copper solution and subsequently, a third layer of selected ligand (0.19 mmol) in methanol (6 mL) was added on top. The test tube was closed and left at room temperature for two weeks. Blue crystals were collected.

Single-crystal X-ray diffraction

Single-crystal X-ray diffraction was performed with a Bruker D8 Venture instrument equipped with a microfocus Mo source (Kα radiation, λ = 0.71073 Å) and a 2D Photon III detector. The main experimental details regarding the structure determination by single-crystal X-ray diffraction are reported in Table S1.† The unit cell was identified and initially refined using APEX4.[48]

Successively, data were integrated and reduced using SAINT[49] and XPREP.[50] Absorption effects were corrected using SADABS.[51] Structures were solved and refined with the aid of SHELXL-2019/1.[52] Hydrogen atoms were fixed at calculated positions and refined by using a riding model. The unit cell of all these materials contains additional total potential solvent accessible void, which is likely to be occupied by highly disordered solvent molecules. These voids have been treated using the SQUEEZE routine of PLATON.[44]

In **UdP-20**, a fixed occupancy value of 0.5 was assigned to the H6 atom and to the CF$_3$ group (C7, F1, F2, F3). Since the complete ligand containing these atoms is generated by symmetry operations, this constraint was applied to preserve the chemical integrity of the structure. Allowing a free variable refinement would lead to an average number of CF$_3$ groups either smaller or larger than one, depending on the refined value. A similar situation occurs in two ligands within the asymmetric unit of **UdP-23**; therefore, the same occupancy value (0.5) was assigned to the hydrogen atoms and methoxy groups bonded to C2 (H2, O1M, C1M, H1MA, H1MB, H1MC) and C23 (H23, O4M, C4M, H4MA, H4MB, H4MC).

Data availability

The data supporting this article such as, PXRD patterns and TGA analysis can be found in the ESI.† CIF files for structural data and AIF files for the adsorption data have been attached as part of the ESI.† Crystallographic data for all the compounds have been deposited at the CCDC under 2411960–2411963 and can also be found attached as part of the ESI.†

Conflicts of interest

The authors declare no competing financial interest.

Acknowledgements

References

1 Y. Liu, L. Chen, L. Yang, T. Lan, H. Wang, C. Hu, X. Han, Q. Liu, J. Chen, Z. Feng, X. Cui, Q. Fang, H. Wang, L. Li, Y. Li, H. Xing, S. Yang, D. Zhao and J. Li, Porous Framework Materials for Energy & Environment Relevant Applications: A Systematic Review, *Green Energy Environ.*, 2024, **9**(2), 217–310, DOI: **10.1016/j.gee.2022.12.010**.

2 L.-X. You, B.-Y. Ren, Y.-K. He, S.-J. Wang, Y.-G. Sun, V. Dragutan, G. Xiong and F. Ding, Structural Features of Lanthanide Coordination Polymers with Catalytic Properties, *J. Mol. Struct.*, 2024, **1304**, 137687, DOI: **10.1016/j.molstruc.2024.137687**.

3 S. Krause, N. Hosono and S. Kitagawa, Chemistry of Soft Porous Crystals: Structural Dynamics and Gas Adsorption Properties, *Angew. Chem., Int. Ed.*, 2020, **59**(36), 15325–15341, DOI: **10.1002/anie.202004535**.

4 A. Wang, Y. Ma and D. Zhao, Pore Engineering of Porous Materials: Effects and Applications, *ACS Nano*, 2024, **18**(34), 22829–22854, DOI: **10.1021/acsnano.4c08708**.

5 R. Singh, G. Singh, N. George, G. Singh, S. Gupta, H. Singh, G. Kaur and J. Singh, Copper-Based Metal–Organic Frameworks (MOFs) as an Emerging Catalytic Framework for Click Chemistry, *Catalysts*, 2023, **13**(1), 130, DOI: **10.3390/catal13010130**.

6 Y. Shen, A. Tissot and C. Serre, Recent Progress on MOF-Based Optical Sensors for VOC Sensing, *Chem. Sci.*, 2022, **13**(47), 13978–14007, DOI: **10.1039/D2SC04314A**.

7 S. G. Subraveti, S. Roussanaly, R. Anantharaman, L. Riboldi and A. Rajendran, How Much Can Novel Solid Sorbents Reduce the Cost of Post-Combustion CO_2 Capture? A Techno-Economic Investigation on the Cost Limits of Pressure–Vacuum Swing Adsorption, *Appl. Energy*, 2022, **306**, 117955, DOI: **10.1016/j.apenergy.2021.117955**.

8 H.-C. J. Zhou and S. Kitagawa, Metal–Organic Frameworks (MOFs), *Chem. Soc. Rev.*, 2014, **43**(16), 5415–5418, DOI: **10.1039/C4CS90059F**.

9 E. R. Engel and J. L. Scott, Advances in the Green Chemistry of Coordination Polymer Materials, *Green Chem.*, 2020, **22**(12), 3693–3715, DOI: **10.1039/D0GC01074J**.

10 G. Férey, Hybrid Porous Solids: Past, Present, Future, *Chem. Soc. Rev.*, 2008, **37**(1), 191–214, DOI: **10.1039/B618320B**.

11 B. Manna, A. V. Desai and S. K. Ghosh, Neutral N-Donor Ligand Based Flexible Metal–Organic Frameworks, *Dalton Trans.*, 2016, **45**(10), 4060–4072, DOI: **10.1039/C5DT03443D**.

12 H. Kajiro, A. Kondo, K. Kaneko and H. Kanoh, Flexible Two-Dimensional Square-Grid Coordination Polymers: Structures and Functions, *Int. J. Mol. Sci.*, 2010, **11**(10), 3803–3845, DOI: **10.3390/ijms11103803**.

13 X. Liu, H. Wang, C. Liu, J. Chen, Z. Zhou, S. Deng and J. Wang, Recent Advances of Multidentate Ligand-Based Anion-Pillared MOFs for Enhanced Separation and Purification Processes, *Chem Bio Eng.*, 2024, **1**(6), 469–487, DOI: **10.1021/cbe.3c00115**.

14 X. Li, H. Bian, W. Huang, B. Yan, X. Wang and B. Zhu, A Review on Anion-Pillared Metal–Organic Frameworks (APMOFs) and Their Composites with the Balance of Adsorption Capacity and Separation Selectivity for Efficient Gas Separation, *Coord. Chem. Rev.*, 2022, **470**, 214714, DOI: **10.1016/j.ccr.2022.214714**.

15 S. Subramanian and M. J. Zaworotko, Porous Solids by Design: $[Zn(4,4'-bpy)_2(SiF_6)]_n \cdot x$ DMF, a Single Framework Octahedral Coordination Polymer with Large Square Channels, *Angew. Chem., Int. Ed. Engl.*, 1995, **34**(19), 2127–2129, DOI: **10.1002/anie.199521271**.

16 Y. Hu, Y. Jiang, J. Li, L. Wang, M. Steiner, R. F. Neumann, B. Luan and Y. Zhang, New-Generation Anion-Pillared Metal–Organic Frameworks with Customized Cages for Highly Efficient CO_2 Capture, *Adv. Funct. Mater.*, 2023, **33**(14), 2213915, DOI: **10.1002/adfm.202213915**.

17 Y. Han, Y. Jiang, J. Hu, L. Wang and Y. Zhang, Efficient C2H2/CO2 and C2H2/C2H4 Separations in a Novel Fluorinated Metal–Organic Framework, *Sep. Purif. Technol.*, 2024, **332**, 125777, DOI: **10.1016/j.seppur.2023.125777**.

18 S. D. Burd, P. S. Nugent, M. H. Mohameda, S. K. Elsaidia and M. J. Zaworotko, Square Grid and Pillared Square Grid Coordination Polymers – Fertile Ground for Crystal Engineering of Structure and Function, *Chimia*, 2013, **67**(6), 372, DOI: **10.2533/chimia.2013.372**.

19 D. Sensharma, D. J. O'Hearn, A. Koochaki, A. A. Bezrukov, N. Kumar, B. H. Wilson, M. Vandichel and M. J. Zaworotko, The First Sulfate-Pillared Hybrid Ultramicroporous Material, SOFOUR-1-Zn, and Its Acetylene Capture Properties, *Angew. Chem., Int. Ed.*, 2022, **61**(8), e202116145, DOI: **10.1002/anie.202116145**.

20 X. Liu, P. Zhang, H. Xiong, Y. Zhang, K. Wu, J. Liu, R. Krishna, J. Chen, S. Chen, Z. Zeng, S. Deng and J. Wang, Engineering Pore Environments of Sulfate-Pillared Metal-Organic Framework for Efficient C_2H_2/CO_2 Separation with Record Selectivity, *Adv. Mater.*, 2023, **35**(20), 2210415, DOI: **10.1002/adma.202210415**.

21 J. Wang, Y. Zhang, P. Zhang, J. Hu, R.-B. Lin, Q. Deng, Z. Zeng, H. Xing, S. Deng and B. Chen, Optimizing Pore Space for Flexible-Robust Metal–Organic Framework to Boost Trace Acetylene Removal, *J. Am. Chem. Soc.*, 2020, **142**(21), 9744–9751, DOI: **10.1021/jacs.0c02594**.

22 B. Song, M. Shivanna, M. Gao, S. Wang, C. Deng, Q. Yang, S. J. Nikkhah, M. Vandichel, S. Kitagawa and M. J. Zaworotko, Shape-Memory Effect Enabled by Ligand Substitution and CO_2 Affinity in a Flexible SIFSIX Coordination Network, *Angew. Chem., Int. Ed.*, 2023, **62**(47), e202309985, DOI: **10.1002/anie.202309985**.

23 B.-Q. Song, Q.-Y. Yang, S.-Q. Wang, M. Vandichel, A. Kumar, C. Crowley, N. Kumar, C.-H. Deng, V. GasconPerez, M. Lusi, H. Wu, W. Zhou and M. J. Zaworotko, Reversible Switching between Nonporous and Porous Phases of a New SIFSIX Coordination Network Induced by a Flexible Linker Ligand, *J. Am. Chem. Soc.*, 2020, **142**(15), 6896–6901, DOI: **10.1021/jacs.0c01314**.

24 Q. Dong, X. Zhang, S. Liu, R. Lin, Y. Guo, Y. Ma, A. Yonezu, R. Krishna, G. Liu, J. Duan, R. Matsuda, W. Jin and B. Chen, Tuning Gate-Opening of a Flexible Metal–Organic Framework for Ternary Gas Sieving Separation, *Angew. Chem., Int. Ed.*, 2020, **59**(50), 22756–22762, DOI: **10.1002/anie.202011802**.

25 D. O'Nolan, A. Kumar and M. J. Zaworotko, Water Vapor Sorption in Hybrid Pillared Square Grid Materials, *J. Am. Chem. Soc.*, 2017, **139**(25), 8508–8513, DOI: **10.1021/jacs.7b01682**.

26 C. Healy, N. C. Harvey-Reid, B. I. Howard and P. E. Kruger, Thermal Decomposition of Hybrid Ultramicroporous

Materials (HUMs), *Dalton Trans.*, 2020, **49**(47), 17433–17439, DOI: **10.1039/D0DT03852K**.

27 P. Zhou, A Porous Cadmium(II) Framework: Synthesis, Crystal Structure, Gas Adsorption, and Fluorescence Sensing Properties: A Porous Cadmium(II) Framework: Synthesis, Crystal Structure, Gas Adsorption, and Fluorescence Sensing Properties, *Z. Anorg. Allg. Chem.*, 2017, **643**(10), 653–656, DOI: **10.1002/zaac.201600448**.

28 L.-W. Lee, T.-T. Luo, C.-M. Wang, G.-H. Lee, S.-M. Peng, Y.-H. Liu, S.-L. Lee and K.-L. Lu, Anion-Induced Structural Transformation of a Sulfate-Incorporated 2D Cd(II)–Organic Framework, *J. Solid State Chem.*, 2016, **239**, 1–7, DOI: **10.1016/j.jssc.2016.03.046**.

29 D. Bradshaw, J. E. Warren and M. J. Rosseinsky, Reversible Concerted Ligand Substitution at Alternating Metal Sites in an Extended Solid, *Science*, 2007, **315**(5814), 977–980, DOI: **10.1126/science.1135445**.

30 A. Dey, A. Garai, V. Gude and K. Biradha, Thermochromic, Solvatochromic, and Piezochromic Cd(II) and Zn(II) Coordination Polymers: Detection of Small Molecules by Luminescence Switching from Blue to Green, *Cryst. Growth Des.*, 2018, **18**(10), 6070–6077, DOI: **10.1021/acs.cgd.8b00924**.

31 J. Liu, H. Shuai, J. Chen, S. Chen, Z. Zhou, J. Wang and S. Deng, Sulfate-Pillared Adsorbent for Efficient Acetylene Separation from Carbon Dioxide and Ethylene, *Chem Bio Eng.*, 2024, **1**(1), 83–90, DOI: **10.1021/cbe.3c00094**.

32 Y. Wen, T. Sheng, Z. Sun, Z. Xue, Y. Wang, Y. Wang, S. Hu, X. Ma and X. Wu, A Combination of the "Pillaring" Strategy and Chiral Induction: An Approach to Prepare Homochiral Three-Dimensional Coordination Polymers from Achiral Precursors, *Chem. Commun.*, 2014, **50**(61), 8320, DOI: **10.1039/c4cc03478c**.

33 D. J. O'Hearn, D. Sensharma, A. Raza, A. A. Bezrukov, M. Vandichel, S. Mukherjee and M. J. Zaworotko, Crystal Engineering of a New Platform of Hybrid Ultramicroporous Materials and Their C_2H_2/CO_2 Separation Properties, *Chem. Sci.*, 2024, **15**(43), 17937–17943, DOI: **10.1039/D4SC03029J**.

34 K. Zou, J. Zhao, C. Liu, Z. Wang and Z. Li, One-Pot Synthesis of Two Magnetic Coordination Polymers with Different Structures Due to the Connectivity of Sulfate Ions, *Eur. J. Inorg. Chem.*, 2013, **2013**(2), 293–298, DOI: **10.1002/ejic.201200706**.

35 Y. Ye, H. Zhang, L. Chen, S. Chen, Q. Lin, F. Wei, Z. Zhang and S. Xiang, Metal–Organic Framework with Rich Accessible Nitrogen Sites for Highly Efficient CO_2 Capture and Separation, *Inorg. Chem.*, 2019, **58**(12), 7754–7759, DOI: **10.1021/acs.inorgchem.9b00182**.

36 S. Mukherjee, N. Sikdar, D. O'Nolan, D. M. Franz, V. Gascón, A. Kumar, N. Kumar, H. S. Scott, D. G. Madden, P. E. Kruger, B. Space and M. J. Zaworotko, Trace CO_2 Capture by an Ultramicroporous Physisorbent with Low Water Affinity, *Sci. Adv.*, 2019, **5**(11), eaax9171, DOI: **10.1126/sciadv.aax9171**.

37 N. Singh and G. Anantharaman, Coordination Polymers Built with Transition Metal Sulphates and Angular 2,5-Bis(Imidazol-1-Yl)Thiophene (Thim₂): Synthesis, Structure and Photoluminescent Properties, *CrystEngComm*, 2014, **16**(27), 6203–6212, DOI: **10.1039/C4CE00691G**.

38 N. Li, J. Pang, F. Lang and X.-H. Bu, Flexible Metal–Organic Frameworks: From Local Structural Design to Functional Realization, *Acc. Chem. Res.*, 2024, **57**(16), 2279–2292, DOI: **10.1021/acs.accounts.4c00253**.

39 A. Schneemann, V. Bon, I. Schwedler, I. Senkovska, S. Kaskel and R. A. Fischer, Flexible Metal–Organic Frameworks, *Chem. Soc. Rev.*, 2014, **43**(16), 6062–6096, DOI: **10.1039/C4CS00101J**.

40 S.-Q. Wang, S. Mukherjee and M. J. Zaworotko, Spiers Memorial Lecture: Coordination Networks That Switch between Nonporous and Porous Structures: An Emerging Class of Soft Porous Crystals, *Faraday Discuss.*, 2021, **231**, 9–50, DOI: **10.1039/D1FD00037C**.

41 Y. H. Andaloussi, D. Sensharma, A. A. Bezrukov, D. C. Castell, T. He, S. Darwish and M. J. Zaworotko, Dinuclear Copper Sulfate-Based Square Lattice Topology Network with High Alkyne Selectivity, *Cryst. Growth Des.*, 2024, **24**(6), 2573–2579, DOI: **10.1021/acs.cgd.4c00094**.

42 G. Bresciani, M. Guelfi, M. Dosa, V. Guiotto, V. Crocellà, M. Lessi and M. Taddei, Cu(II)-Based Coordination Polymers Containing 1,4-Bis(1*H*-Imidazol-1-Yl)Benzene and Monovalent Fluorinated Anions, *Cryst. Growth Des.*, 2024, **24**(21), 8999–9010, DOI: **10.1021/acs.cgd.4c01038**.

43 *The IUPAC Compendium of Chemical Terminology: The Gold Book*, ed. V. Gold, International Union of Pure and Applied Chemistry (IUPAC), Research Triangle Park, NC, 4th edn, 2019, DOI: **10.1351/goldbook**.

44 A. L. Spek, PLATON SQUEEZE: A Tool for the Calculation of the Disordered Solvent Contribution to the Calculated Structure Factors, *Acta Crystallogr., Sect. C: Struct. Chem.*, 2015, **71**(1), 9–18, DOI: **10.1107/S2053229614024929**.

45 K. Koupepidou, V. I. Nikolayenko, D. Sensharma, A. A. Bezrukov, M. Shivanna, D. C. Castell, S.-Q. Wang, N. Kumar, K. Otake, S. Kitagawa and M. J. Zaworotko, Control over Phase Transformations in a Family of Flexible Double Diamondoid Coordination Networks through Linker Ligand Substitution, *Chem. Mater.*, 2023, **35**(9), 3660–3670, DOI: **10.1021/acs.chemmater.3c00334**.

46 G. R. Fulmer, A. J. M. Miller, N. H. Sherden, H. E. Gottlieb, A. Nudelman, B. M. Stoltz, J. E. Bercaw and K. I. Goldberg, NMR Chemical Shifts of Trace Impurities: Common Laboratory Solvents, Organics, and Gases in Deuterated Solvents Relevant to the Organometallic Chemist, *Organometallics*, 2010, **29**(9), 2176–2179, DOI: **10.1021/om100106e**.

47 V. Crocellà, C. Atzori, G. Latini and M. Signorile, A Kit for Volumetric Measurements of Gas Adsorption. PCT/IB2021/051769, WO2021/181211A12021, 2021.

48 Bruker, *APEX4 V2021.10-0*, Bruker AXS Inc., Madison, Wisconsin, USA, 2021.

49 Bruker, *SAINT v8.30A*, Bruker AXS Inc., Madison, Wisconsin, USA, 2012.

50 Bruker, *XPREP V2014/2*, Bruker AXS Inc., Madison, Wisconsin, USA, 2014.

51 Bruker, *SADABS V2016/2*, Bruker AXS Inc., Madison, Wisconsin, USA, 2016.

52 G. M. Sheldrick, *SHELXL-2019/1*, Bruker AXS Inc., Madison, Wisconsin, USA, 2019.